# Simple Fabrication of Polyvinylidene Fluoride/Graphene Composite Membrane with Good Lipophilicity for Oil Treatment

Murong Yang, Kaikai Chen,* Mianning Wang, Huanhuan Chen, Haoyang Ling, Wei Zhao, Haihui Liu, and Changfa Xiao*

ACCESS | 📊 Metrics & More | 📑 Article Recommendations | 🆂🆘 Supporting Information

**ABSTRACT:** Graphene (GE) is an emerging type of two-dimensional functional nanoparticle with a tunable passageway for oil molecules. Herein, polyvinylidene fluoride (PVDF)/GE composite membranes with controllable pore structure were fabricated with a simple non-solvent-induced phase separation method. The change of crystallinity and crystal structure ($\alpha$, $\beta$, $\gamma$, etc.) generated is due to the addition of GE, which benefits the design of a suitable pore structure for oil channels. Meanwhile, the hydrophobicity and thermal stability of the composite membrane were obviously enhanced. With 3 wt % GE, the contact angle was 124.6°, which was increased greatly compared to that of the GE-0 sample. Moreover, the rate of the phase transition process was affected by the concentration of casting solution, temperature, and composition of the coagulation bath. For example, the composite membrane showed better oil−water separation properties when the coagulation bath was dioctyl phthalate. In particular, the oil flux and separation efficiencies were up to 2484.08 L/m$^2$·h and 99.24%, respectively. Consequently, PVDF/GE composite membranes with excellent lipophilicity may have good prospects for oily wastewater treatment.
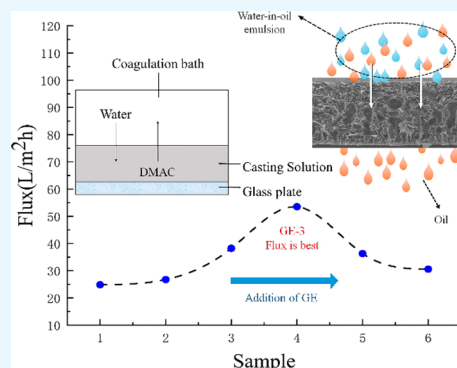
## 1. INTRODUCTION

Today, the oil industry continues to play an important role, as the leakage of crude oil has caused catastrophic harm to ecosystems, not only causing irreparable losses of economic but also seriously threatening aquatic organisms and even human survival.[1−3] Additionally, the terrestrial ecosystem was threatened by the discharge of oily wastewater and organic solvents, such as dyed wastewater, emulsified wastewater, and so on.[4] How to remove oily wastewater effectively and quickly has attracted widespread attention. Therefore, the development of techniques for oil−water separation has become an emerging issue.[5,6] Various traditional techniques, including physical adsorption or separation,[7−10] chemical reaction,[11] biodegradation,[11,12] or centrifugal sedimentation,[13] are devoted to treating the oily wastewater field. However, these methods always require high energy consumption.[14,15] Therefore, the development of satisfactory technology for oil−water separation is urgently needed.

Membrane separation technology has unique characteristics, including (1) being environmentally friendly and energy-efficient, (2) having a small usable area and relatively simple operation process,[16−18] and (3) having excellent separation properties and long-term stability.[19] Therefore, membrane separation technology has shown broad developmental prospects.[18] Polymeric membranes play an important role in membrane separation technology due to the advantages of easy preparation, flexibility, and low cost.[20−22] Presently, poly-

vinylidene fluoride (PVDF), cellulose acetate (CA), and polysulfone (PSF) have been employed to prepare membranes.[23−26] Among them, PVDF is regarded as a potential oil−water separation membrane material due to its high C−F bond energy (486 kJ/mol) and low surface energy, exhibiting good chemical resistance and excellent thermal stability and hydrophobicity. Generally, the PVDF membrane could be prepared with a non-solvent-induced phase separation (NIPS) method, melt spinning, or an electrospinning technique. Up to now, yhe commonly used membranes in the market were prepared with the NIPS method due to the advantages of having a controllable pore structure. However, these membranes appeared to have an inefficient oil−water separation property because the forming hydrated layer on the membrane surface prevents oil penetration.[27,28] Therefore, the improvement of lipophilicity on the PVDF membrane surface that could be built by the introduction of functional nanomaterials including carbon nanotubes, inorganic nanoparticles, and graphene (GE) in the surface morphology of modified PVDF membranes is important. Recently, GE as an

emerging type of two-dimensional functional nanoparticle has received increasing attention.[29−31] For instance, it was found that the incorporation of GE could significantly increase the hydrophobicity of polymers.[32]

In 2016, Wu et al. fabricated a PVDF membrane with the NIPS method, and to enhance the hydrophobicity of the membranes, they added graphene nanosheets into the PVDF membranes and applied the membrane to the contactor absorption of $CO_2$.[33] Yuan et al. added GE to the polymer membrane to improve the hydrophobicity and breaking strength of the membrane, and this hybrid membrane can be used for oil−water separation. However, how GE affects the lipophilicity of membranes to enhance oil flux was not studied.[34] Actually, the addition of GE could improve the hydrophobicity and lipophilicity of the membranes at the same time, which could increase the oil permeability in the oil−water separation. A super-lipophilic and an under oil super-hydrophobic PVDF/GE composite nanofibrous membrane was fabricated through an electrospinning strategy by Zhang et al. The membrane shows good separation ability and controllable pore structure with the only variable of GE content.[35]

As far as we know, there has been little research illustrating the change of oil flux in terms of different coagulating bath conditions during the fabrication of PVDF membranes. In this research, the PVDF membrane with different GE contents was prepared with a simple method and then immersed in a coagulation bath of cold water, hot water, and dioctyl phthalate (DOP). The objective of the PVDF/GE membrane to improve lipophilicity with a controllable pore structure was also evaluated.

## 2. MATERIALS AND METHODS

**2.1. Materials.** PVDF (solef 6010) was purchased from Trump Chemical Corp. (Wuxi, China). Knano Graphene Technology Co., Ltd., (Xiamen, China) offered GE (1−3 layers, layer size ≈5−8 $\mu$m). Kermel Chemical Reagent Co., Ltd. (Tianjin, China) and Heshilian Chemical Co., Ltd. (Tianjin, China) provided DOP, *N*,*N*-dimethylacetamide (DMAc), ethanol, and kerosene. In this study, analytical grade chemical reagents were used.

**2.2. Preparation of the PVDF/GE Membrane.** The simple NIPS method was utilized to prepare PVDF/GE membranes. The process generally involved the casting solution being extended on the dry glass plate and then rapidly immersed into nonsolvent. During this process, the solvent and nonsolvent generated double diffusion. After a while, the double diffusion between the solvent and the nonsolvent (the solvent is DMAc, and the nonsolvent is water or DOP) reached a certain level, and the casting solution became a thermodynamically unstable solution, and liquid−liquid separation or liquid−solid separation crystallization occurred, which became two phases called the rich and poor phase. Generally, the main body of the membrane and the so-called pores were produced by rich and poor phases, respectively. GE with different contents (0, 0.5, 2, 3, 4, and 5 wt %) was dispersed first in the solvent mixed with DMAc and DOP and are named GE-0, GE-0.5, GE-2, GE-3, GE-4, and GE-5, respectively. The specific composition is shown in Table 1. The mixture solution was sealed and underwent ultrasonic treatment for 9 h in a JP-080s ultrasound machine to form an oily layer on the surface of GE and the mixture solution more evenly. Then the prepared casting solution with

**Table 1. Content of Casting Solutions**

| sample | DOP (wt %) | GE (wt %) | PVDF (wt %) | DMAc (wt %) |
|--------|-----------|-----------|-------------|-------------|
| GE-0   | 10        | 0         | 13          | 77          |
| GE-0.5 | 10        | 0.5       | 13          | 76.5        |
| GE-2   | 10        | 2         | 13          | 75          |
| GE-3   | 10        | 3         | 13          | 74          |
| GE-4   | 10        | 4         | 13          | 73          |
| GE-5   | 10        | 5         | 13          | 72          |

PVDF addition was obtained under the condition of a water bath at 70 °C for 4 h. In the casting solution, PVDF could produce a greater force with the molecules of oily particles due to the F-containing molecular chain. Finally, a homogeneous casting solution of GE was formed after 1 h of defoaming treatment. The membrane was prepared by scraping it onto a glass plate with 200 $\mu$m thickness. Then the as-prepared casting solution was immediately put into a cold water (15 °C), DOP, and hot water (80 °C) coagulation bath to form the membrane. The preparation flowchart of the samples is demonstrated in Figure 1. The prepared membranes were stored in distilled water for about 24 h for extraction treatment before being dried (the membrane in the DOP coagulation bath was first immersed in alcohol for 15 min to remove DOP on the surface and then immersed in distilled water).

**2.3. Membrane Characterization.** *2.3.1. Scanning electron Microscopy and Confocal Scanning Microscopy.* The surface morphology and cross-sectional GE distribution of the membranes were characterized by Netherlands Phenom XL scanning electron microscopy (SEM). Particularly, the cross-sectional morphologies were obtained by freezing the PVDF/GE membranes in liquid nitrogen and breaking them with tweezers. In addition, in order to obtain a sharper morphology, a layer of gold needs to be sprayed. Under stable temperature and humidity conditions, the three-dimensional (3D) morphologies and average roughness parameters ($R_a$) of PVDF/GE membranes were analyzed by confocal scanning microscopy (CSM, Germany).

*2.3.2. Mechanical Properties.* The electronic tensile testing machine (JBGW-400, China) was utilized to evaluate the mechanical properties of the membranes, including tensile stress and elongation at break. Three tests were required to reach the average value of the mechanical properties.

*2.3.3. X-ray Diffraction and Fourier Transform Infrared Spectroscopy.* The crystal phase change in the PVDF membranes was analyzed by an X-ray diffractometer (D8 ADVANCE, Germany). The generator runs at room temperature at 60 kV and 80 mA. The scanning range was 5−60° ($2\theta$), and the step size was 0.02°. The Fourier transform infrared (FTIR) spectrum was recorded with a Thermo-Scientific FTIR instrument (Nicolet iS50, USA).

*2.3.4. Differential Scanning Calorimetry and Thermogravimetric Analysis.* In order to explore the influence on curing temperature with GE addition on PVDF, a differential scanning calorimetry (DSC) (DSC200F3, Germany) test was carried out on a PVDF membrane, and the curing temperature curve was obtained when the heating rate was 10 °C/min in the presence of nitrogen. The influence of GE content on the apparent crystallinity ($X_m$) of the samples could be evaluated as follows (eq 1):

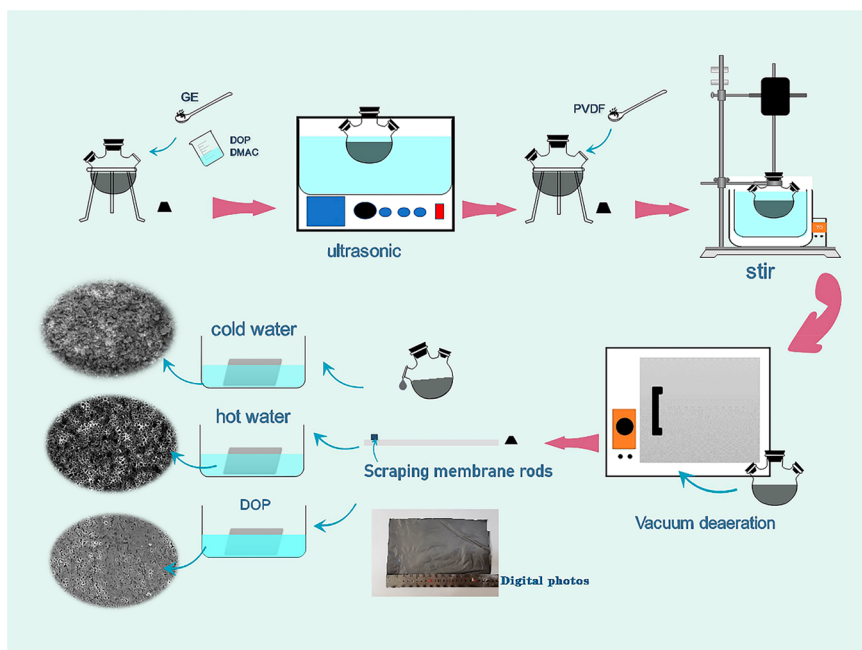$$X_m = \frac{\Delta H_m}{(1 - \omega)\Delta H_m^*} \tag{1}$$

**Figure 1.** Preparation schematic of PVDF/GE membranes. Photograph courtesy of Murong Yang.

where the melting enthalpy (104.5 J/g)[21] of the 100% crystalline PVDF was represented by $\Delta H_m^*$ and the weight fraction of PVDF in the samples was represented by $\omega$.

To study the thermal stability of the membranes, thermogravimetric analysis (TGA) (STA449F3, Germany) was used to study the thermogravimetric loss (nitrogen atmosphere) of the membrane.

*2.3.5. Pore Size Distribution and Porosity.* To analyze the pore size distribution of the membranes, three samples were randomly cut from the prepared membranes and measured with a capillary flow pore size analyzer (BSD-PB, China).

The samples were soaked in *n*-butyl alcohol for 24 h. Then excess liquid was wiped off from the surfaces with filter paper and immediately weighed to determine the wet mass ($m_{wet}$, g). After being dried at 40 °C in oven for 24 h, the dry mass of the membrane samples ($m_{dry}$, g) was weighed. The porosity ($\varepsilon$, %) was calculated using eq 2.[22]

$$\varepsilon = \frac{m_{wet} - m_{dry}}{\rho_G V} \times 100\% \qquad (2)$$

where the density of *n*-butyl alcohol (0.81 g·cm$^{-3}$) was represented by $\rho_G$; the polymer density (1.78 g·cm$^{-3}$) is represented by $\rho_P$, and the volume of the wet membrane sample is represented by $V$.

*2.3.6. Contact Angle.* In order to study the hydrophobicity and lipophilicity of the membranes, dynamic contact angle measurements were performed on the upper and lower surfaces of the prepared membranes using a DSA-100 contact angle goniometer (KRUSS, Germany). Values from at least five different locations were taken on the same surface, and the average was calculated. The contact angles of oil, water, and water in oil were measured. The water contact angle in oil was determined by pouring kerosene into a glass container and then the membrane placed into kerosene to measure the contact angle of water droplets in kerosene with the membrane.

**2.4. Water-in-Oil Properties.** *2.4.1. Water-in-Oil Emulsion.* Generally, 0.1 g of Span 80 (HLB = 4.3) (HLB is

hydrophile lipophilic balance) was gradually dissolved in 99 mL of kerosene under stirring conditions. Then 1 g of deionized water was added to the kerosene (0.2 g every 30 min for a total of five additions). After 1 g of deionized water was added, the mixture was stirred for another 5 h to form a milky emulsion. The prepared emulsion was uniform without obvious precipitation or agglomeration.

*2.4.2. Separation Experiment.* The water-in-oil emulsion separation experiments were carried out under certain pressure. Each sample was pressed between the self-made suction filtration device (effective membrane sample area = 1256 mm$^2$), and a piece of filter paper was placed under the sample to prevent the membrane from being damaged. The water-in-oil emulsion was poured into the device, and the filtrate was passed through the membrane sample at a pressure of 0.085 MPa and collected into a suction flask. The permeation flux for each sample was record every 5 min and calculated according to eq 3:

$$J = \frac{V}{St} \qquad (3)$$

where the permeation flux (L/m$^2$·h) is represented by $J$, the volume of collected filtrate (L) is represented by $V$, the effective area of the sample (m$^2$) and the operation time (h) are represented by $S$ and $t$, respectively. In addition, the water content of filtrate was measured with a Karl Fischer moisture titrator (C20, Mettler Toledo). The filtrate was drawn into a 0.1 mL syringe and injected into a Karl Fischer moisture titrator; after the electrolyte reached equilibrium and the water content was read, at least three groups of filtrate measurements were calculated. The oil/water separation efficiency could be calculated using eq 4:

$$E = \frac{C_1 - C_2}{C_1} \times 100\% \qquad (4)$$

where the oil/water separation efficiency (%) is represented by $E$. The water content in water-in-oil emulsion and water content in filtrate are represented by $C_1$ and $C_2$, respectively.
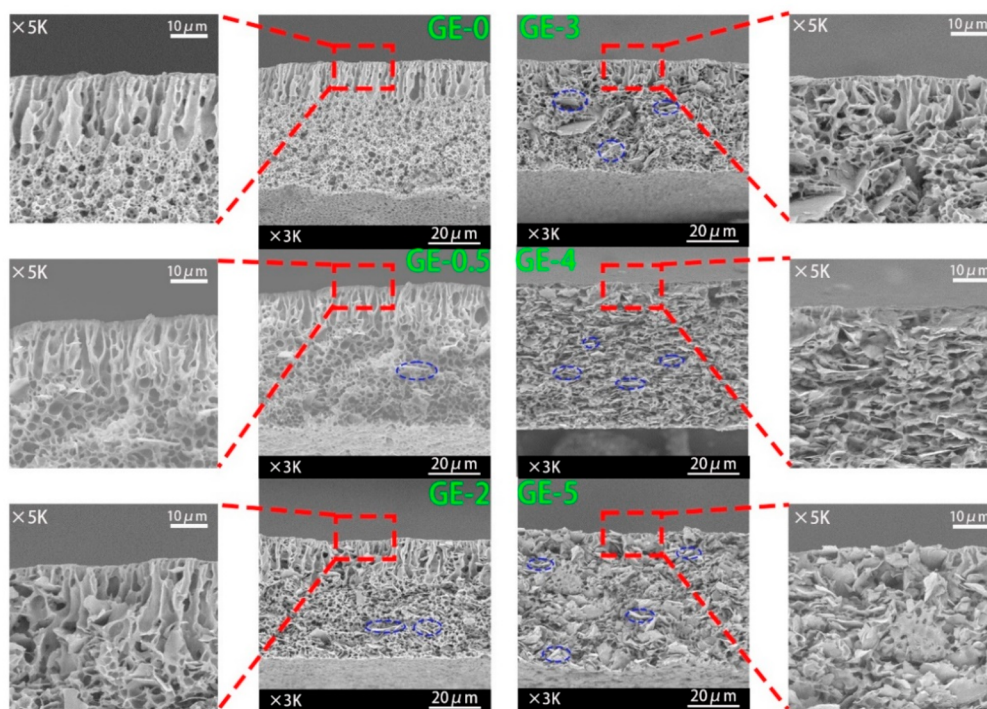
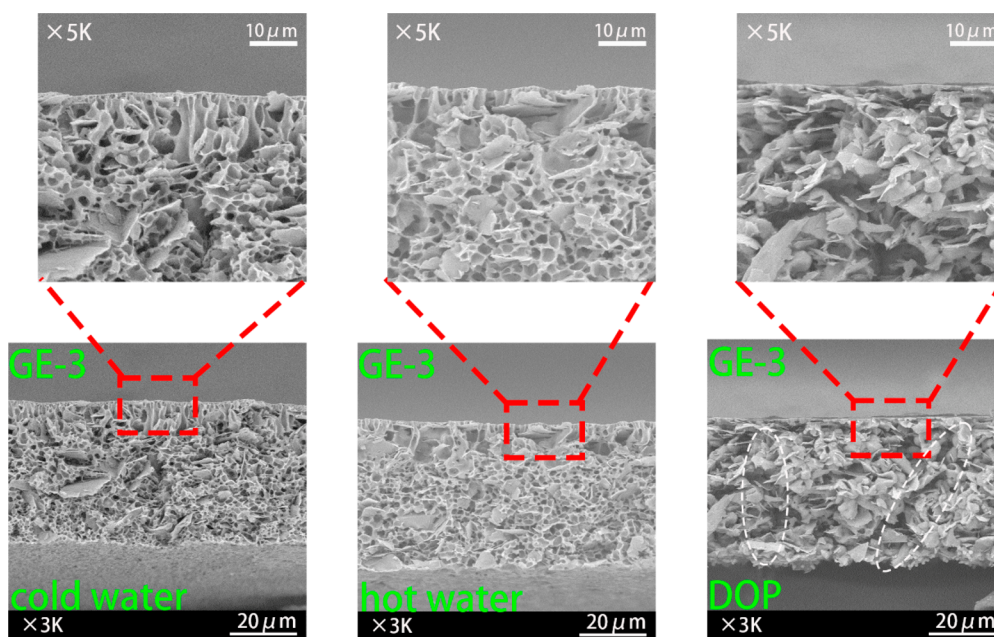**Figure 2.** Cross-sectional SEM morphology of the PVDF/GE sample.



**Figure 3.** SEM image of the PVDF/GE membrane in different coagulation baths.

All of the experiments were performed at least three times and averaged.

**2.5. Oil Permeation Flux.** Generally, the lipophilicity of the membrane was determined by measuring the permeation flux of pure oil. Three sample slices with a diameter of more than 40 mm were cut randomly from the prepared membrane. The flux of each sample was measured every 5 min and measured at least three times to get the average value calculated with eq 3.

In order to better apply the membrane to the treatment of oily wastewater, we further measured the flux of the oil slick.

By tilting the filtration device to 40°, kerosene was poured into the device first (in order to distinguish water from oil, the kerosene was dyed with SudanIII), and then 20 mL of water was added, with water and oil each taking up half of the membrane area. Flux was measured every 5 min at least three times to get the average value calculated with eq 3.

## 3. RESULTS AND DISCUSSION

**3.1. Membrane Structure.** In general, the cross-sectional morphology of PVDF/GE membranes could be visually observed to illustrate the change of pore structure by
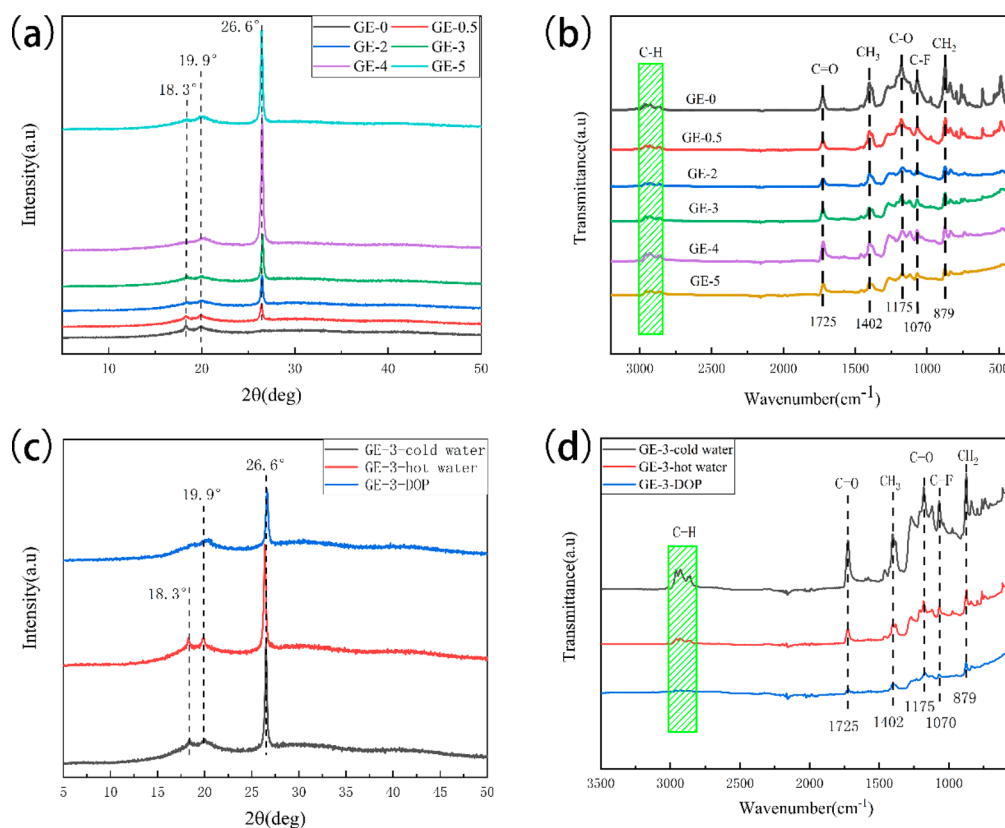
**Figure 4.** (a,c) XRD of PVDF/GE membranes with different graphene contents and different coagulation baths. (b,d) FTIR spectra of PVDF/GE membranes with different graphene contents and different coagulation baths.

introducing GE. As mentioned above, the transient and delayed liquid−liquid separation occurs in the double diffusion process (transient liquid−liquid phase separation was rapid separation and formed an asymmetrical membrane with a thin cortex and a porous structure; delayed liquid−liquid phase separation usually obtained thick and dense cortex and spongy sublayer structures). As shown in Figure2, the number of graphene sheets could be clearly observed on the cross section, and the graphene sheets were evenly dispersed. It was proven that the operation of adding GE into the solvent for 9 h of ultrasound was useful. The cross section of the pure PVDF membrane consists of a cortical, finger-like pore and cellular structure. The finger-like pores become cellular with the increased content of GE due to the delayed liquid−liquid phase separation. Moreover, the cellular pores in the graphene sheets gradually coalesce, forming GE oil channels. This was because the concentration of casting solution gradually increases with the increase of graphene content, which would increase the size of cellular pores and decrease the generation of macroporous structures in the membrane.[36] The cortex of the membrane was thickened, which can be seen in the enlarged image. Meanwhile, porosity was measured, and the specific value is shown in Table S1.

One of the important factors was a change of the coagulation bath that affects the phase conversion rate to change the pore structure. Figure3 shows the SEM images of PVDF/GE membranes under different coagulation baths. As shown in these figures, the finger-like pores formed in cold water were relatively uniform, and most of the cellular structures were closed. Only the cellular structures containing graphene sheets were interpenetrating. When the coagulation bath was hot

water, the transient liquid−liquid phase separation occurred. At the same time, the finger-like pore became smaller, and a larger pore was formed between the finger-like pore and the cellular pore. When the coagulation bath was DOP, the delayed liquid−liquid phase separation was generated and the phase conversion rate slowed down. The uniform cellular structures in the cross section interconnect with each other, forming obvious GE oil channels. Because there was DOP in the solvent, when the casting solution was immersed in DOP, the surface would not form a thicker layer. This kind of pore structure was a benefit for oil−water separation.

Figure 4a,c shows the XRD images of the prepared PVDF membranes. In the diffraction pattern of the original PVDF membrane, the peaks appeared at 18.5 and 20.1° (2θ), respectively, corresponding to the γ-type characteristic peaks of PVDF. In the diffraction pattern of the PVDF/GE composite membranes, new peaks appeared at 2θ = 26.6°, corresponding to the α-type characteristic peaks of PVDF. So, the incorporation of GE seems to lead to the transformation of PVDF crystals from γ- to α-type during the phase transition. The diffraction peak intensity at 2θ = 19.9° was due to the enhancement of the crystalline region of the PVDF/GE membrane. For instance, a study reporting the original PVDF and PVDF/GE composite membranes also showed the same observations.[24] The addition of GE affected the polymorphism of PVDF and favored the formation of a β-phase. At 2θ = 26.6°, the diffraction peaks of PVDF/GE weaken, mainly due to the formation of a β-phase in the PVDF/GE crystalline region.[25−27] The presence of a β-phase weakened the toughness of the membranes.
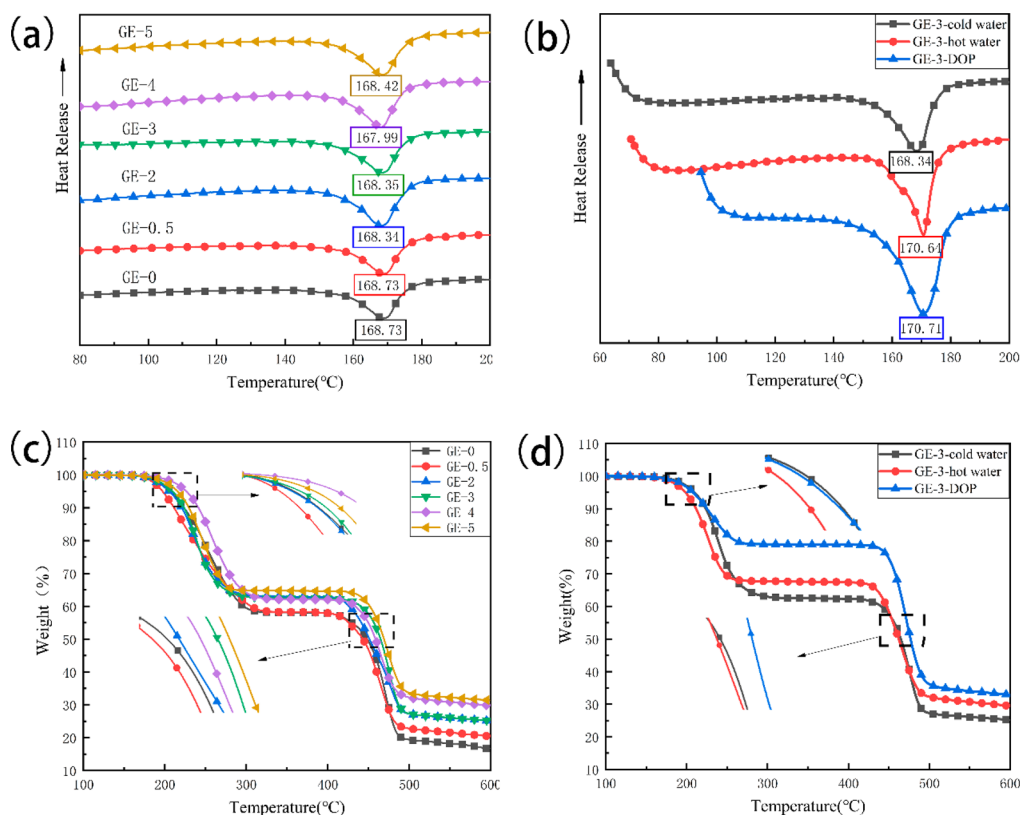
**Figure 5.** (a,c) DSC thermograms and TGA of PVDF/GE membranes with different graphene contents. (b,d) DSC thermograms and TGA of PVDF/GE membranes with different coagulation baths.

The surface functional groups of PVDF/GE membranes were evaluated by FTIR spectroscopy. The peaks of the six samples were similar, as can be seen from Figure 4b. The stretching vibration peak of C−H appeared between 2800 and 3000 cm$^{-1}$; the peak of C=O was located at 1725 cm$^{-1}$, and the peak of CH$_3$ arose at 1402 cm$^{-1}$. The peak did not change with GE content. The peak of C−O emerged at 1175 cm$^{-1}$; the peak of C−F came out at 1070 cm$^{-1}$, and the peak of CH$_2$ appeared at 879 cm$^{-1}$. All three peaks weaken slightly with increasing GE content. As can be seen from Figure 4d, there was no new bond formation in the altered coagulation bath. However, compared with the membrane formed in cold water, the peak value was obviously weakened when the coagulation bath contained hot water and DOP. The results show that GE was dispersed in the membrane uniformly because no new bonds were formed during the preparation of PVDF/GE membranes.

Meanwhile, the crystallization process of PVDF/GE membranes was studied. DSC thermograms of the pure PVDF and PVDF/GE membranes are shown in Figure 5a,b. The results show that, with the increase of GE content, the temperature increase range of the melt broadens, and the peak temperature slightly shifts to low temperature with the increase of GE content. Compared with pure PVDF, the melting temperature of the composite membranes with higher GE content was slightly lower, which may be related to the thin crystals formed during the melt crystallization process, and that the wider range of melt absorption was caused by the broader distribution in thickness of PVDF α-type crystals developed in the composite membranes.[17] After the coagulation bath was changed, when the coagulation bath was DOP, the melting endothermic peak was the widest and the melting temperature

was the highest. Changes in the coagulation bath may result in a slower rate of transition from γ to α during phase separation. Considering the difference in GE content in PVDF/GE membranes, the apparent crystallinity ($X_m$) of composites could be calculated with eq 1. Peak melting temperature ($T_m$), enthalpy ($\Delta H_m$), and apparent crystallinity ($X_m$) were calculated and arranged in Table S2. Furthermore, the apparent crystallinity ($X_m$) of all composite membranes was almost the same, within the experimental error range, without changing the coagulation bath. It was reasonable to believe that the dispersed GE sheets in the PVDF/GE membrane accelerated the formation of α-phase crystals and the overall melting crystallization rate of PVDF. When the coagulation bath was DOP, the apparent crystallinity increased obviously. Therefore, the membrane formation in DOP slowed down the formation of α-phase crystals and also shortened the overall melting crystallization rate of PVDF.

To explore the thermal stability of the membranes, the thermogravimetric analyzer was used to study the thermogravimetric loss of PVDF/GE membranes. Figure 5c,d presents a graph of TG curves of samples under the N$_2$ atmosphere condition. As shown, the typical weightlessness temperatures ($T_{5\%}$ and $T_{50\%}$) for 5 and 50% weight loss for all samples were observed from the TG curves, as summarized in Table S3. We could see from the table that the temperature of the GE-0 sample with weight loss of 5% was 205.74 °C. The temperature of weight loss of 50% was at 447.26 °C, and the carbon residual rate of 600 °C was 16.73%. The temperature of the membrane at 5 and 50% weight loss increased with the increase of GE content; some decreased within the allowable error range, and the carbon residue rate was increased every time. When the content of GE was 5 wt %, at the temperature
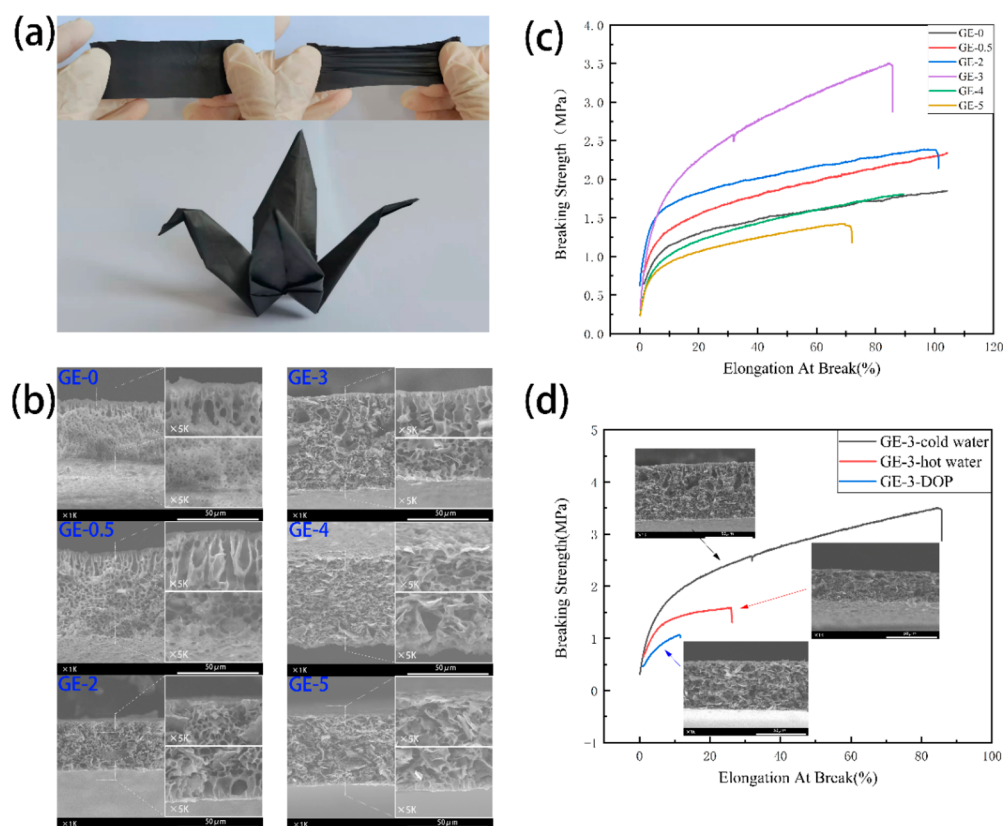
**Figure 6.** (a) Membrane digital photograph. (b) SEM image of PVDF/GE membrane cross section. (c) Strain−stress curves with different GE content. (d) Strain−stress curves with different coagulation baths. Photograph courtesy of Murong Yang.

of 5 and 50% of weightlessness, the carbon residual rate was the maximum. It was shown that the higher the content of GE, the more the cross-linking network structure formed in the membrane and the better the stability of the membranes. To further characterize the thermal stability of PVDF/GE membranes in different coagulation baths, the weight loss rate of the membranes at 5 and 50% and the carbon residual rate at 600 °C were determined and are summarized in Table S4. It was found that the thermal stability of the membrane formed in cold water and hot water presented not much difference, and the membrane formed in DOP exhibited the best thermal stability.

**3.2. Mechanical Properties of Membranes.** Generally, the actual operation of membranes could be evaluated by the mechanical properties. To characterize the mechanical property of the membranes, the tensile strength was determined. The results are shown in Figure 6 in detail. A certain tensile force was applied to the PVDF/GE membranes, as shown in Figure 6a. As can be seen from the SEM image in Figure 6b, the content of graphene was 4 and 5 wt %, and a layered structure on the cross section gradually formed. As shown in Figure 6c, the increasing content of GE improved the breaking strength of the membranes to some extent. However, when the content of GE increased to 4 and 5 wt %, the breaking strength decreased. Therefore, it could be determined that a layered structure was not conducive to the tensile properties of the membranes. Meanwhile, the elongation at the break decreased with the increase of graphene content, as also observed. The results showed that the PVDF/GE membranes exhibited the best mechanical strength when the GE content was 3 wt %.

The mechanical strength of PVDF/GE membranes containing 3 wt % GE in different coagulation baths was further studied, as shown in Figure 6d. When the coagulation bath was hot water, the breaking strength of the membrane and the elongation at break was significantly reduced. It could be found from the SEM images that the cross section of the membranes formed in DOP was a completely layered structure. This layered structure reduced strain and stress of the membrane. This maybe produced the "trade-off" effect for achieving the good membrane performance and high oil flux.

**3.3. Hydrophobic PVDF/GE Membrane.** The contact angle was usually affected by the surface roughness of the hydrophobic membrane. Figure 7a,c,e shows the top surface of PVDF/GE membranes in different GE contents and different coagulation baths, and Figure 7b,d,f shows the 3D images of their CSM. The surface pores of the pure PVDF membrane were small and evenly distributed. With the increase of the content of GE, more graphene sheets could be observed on the surface, and the pores became larger and distributed unevenly. The surface roughness also increased gradually. After the coagulation bath was changed, it could be seen that the largest pores are formed in hot water and the corresponding surface roughness value was the largest. The membrane surface formed in DOP was relatively dense. The roughness of the top and bottom surfaces emerged different because the bottom surface was in direct contact with the glass plate. As shown in Figure S1, the pore size of the lower surface is larger than that of the upper surface, and the surface roughness value was also larger than that of the top surface.

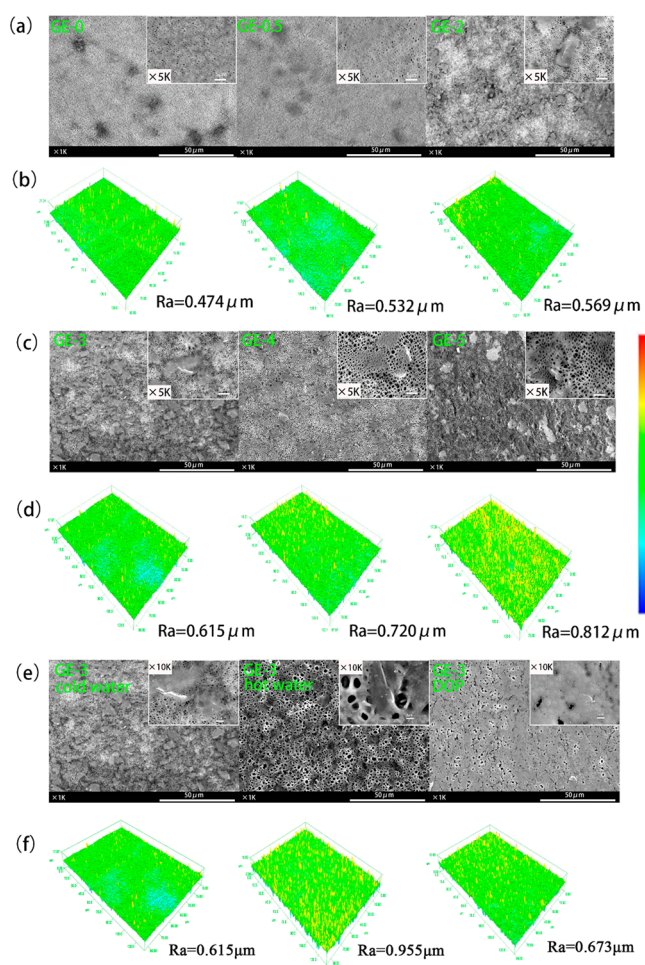The hydrophobicity of the top and bottom surface of PVDF/GE membranes was different with the increased

**Figure 7.** Top surface SEM and CSM images of PVDF/GE membrane. (a,c) SEM images of different GE content of PVDF/GE membranes. (e) SEM image of different coagulation bath PVDF/GE membranes. (b,d) CSM images of different GE content PVDF/GE membranes. (f) CSM image of different coagulation bath PVDF/GE membranes.

content of GE, and the contact angle of the top surface gradually increases. However, the contact angle of the bottom surface reached a maximum of 124.6° when the GE content was 3 wt %, then it decreased with the increase of GE content. The reason for this was that the pore size of the bottom surface

increased as the GE sinks and stacks, and the surface tension decreased. The hydrophobicity of GE containing 3 wt % membranes in different coagulation baths was further studied. As shown in Figure 8a,b (samples 1, 2, and 3 indicates that the coagulation bath was cold water, hot water, and DOP, respectively), the contact angles on both surfaces of the PVDF/GE membrane samples were consistent with the $R_a$ values in the CSM images. The top surface has a maximum contact angle of 116° in hot water, and the bottom surface has a maximum contact angle of 132.7° in DOP.

**3.4. Application of PVDF/GE Membrane.** The separation performance of the membrane was investigated by a water-in-oil experiment. The water-in-oil emulsion prepared by us was slowly poured into the glass device, and a pressure of 0.085 MPa was exerted on the membrane (Figure 9a). The oil droplets were observed to be collected in the bottom suction flask; the oil permeation flux was recorded every 5 min, and the flux was calculated using eq 3. In order to determine whether there was water passing through, a trace moisture meter formulated a measurement of the filtrate, and eq 4 was used to calculated the rejection rate of the filtrate. The results were recorded together in Figure 9b. It can be seen from the figure that the flux first increases and then decreases with the increased content of GE. When the GE content was 3 wt %, the maximum permeation flux was 53.50 L/m$^2$·h, and the rejection rate was 99.28%. To illustrate this phenomenon, the membrane's contact angle with water in oil was also measured, as shown in Figure 9c. With the increase of GE content, the contact angle of water in kerosene also showed a trend of first increasing and then decreasing. When the GE content was 3 wt %, the contact angle reached the maximum value. Therefore, addition of GE to the PVDF membrane could improve the oil−water separation ability of the membrane to a certain extent.

The oil−water separation capacity of the membranes formed in different coagulation baths was measured at a pressure of 0.01 MPa. The water contact angle in the oil of the membrane formed in hot water and DOP was greater than that formed in cold water, as could be seen in Figure 9e. According to the flux figure (Figure 9d), the membrane flux formed in DOP was the best, reaching 39.17 L/m$^2$·h. Compared to the membrane formed in cold water, the separation capacity was more than doubled, and the rejection rate reached more than 99%. According to the previous rule, flux increased with the water contact angle in oil. The membrane oil flux formed in hot
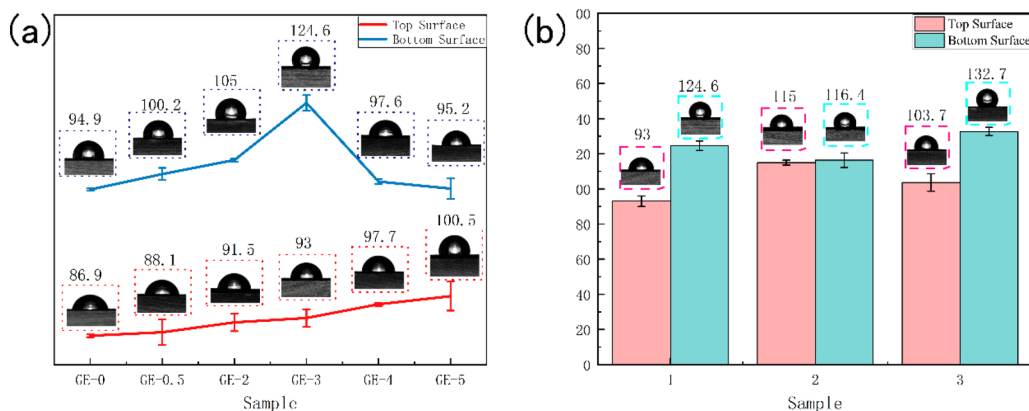


**Figure 8.** (a) Hydrophobicity of PVDF/GE membranes with different graphene contents. (b) Hydrophobicity of PVDF/GE membranes with different coagulation baths.
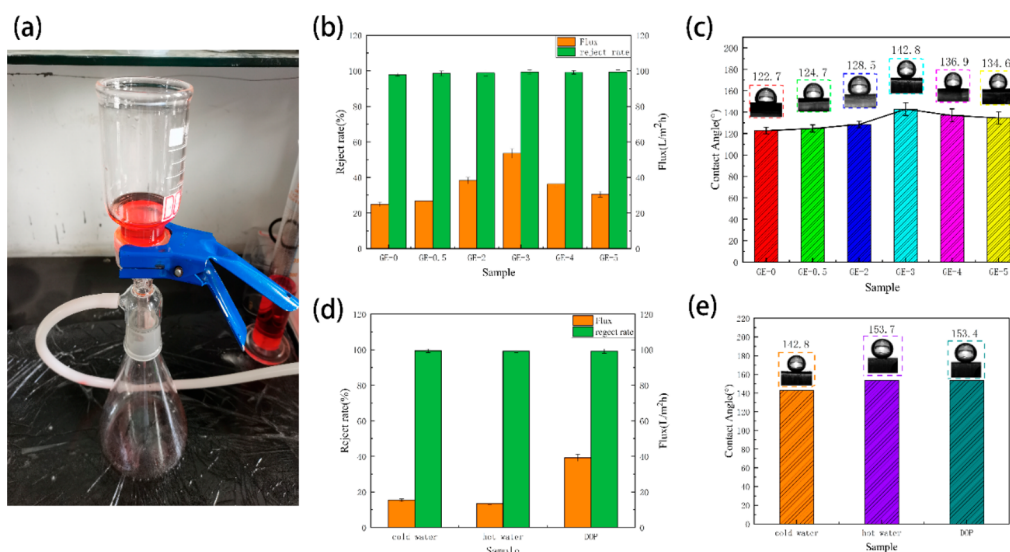
**Figure 9.** (a) Flux device figure. (b) Oil-in-water flux and rejection rate diagram with different graphene contents. (c) Membrane contact angle with water in oil with different graphene contents. (d) Oil-in-water flux and reject rate diagram with different coagulation baths. (e) Membrane contact angle with water in oil with different coagulation baths. Photograph courtesy of Murong Yang.
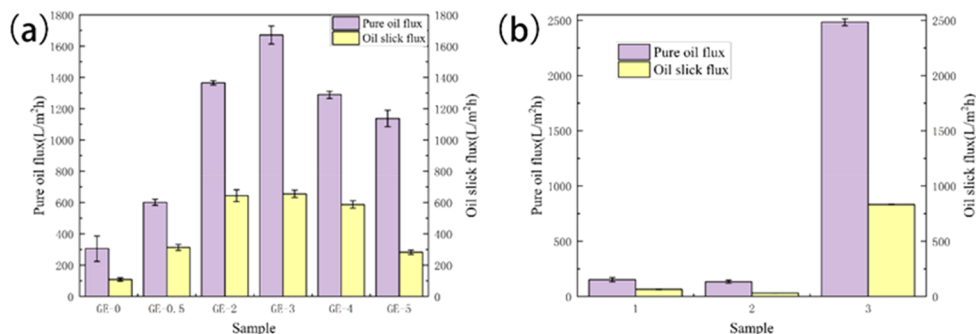


**Figure 10.** (a) Flux diagrams of pure oil and oil slick with different graphene contents. (b) Flux diagrams of pure oil and oil slick with different coagulation baths.

water should be larger than that formed in cold water, but the experimental results were contrary. We speculated that it was related to the pore size distribution inside the membrane, and the detailed analysis will be explained later.

To illustrated the lipophilicity of PVDF/GE membranes, the flux of pure oil was tested. The pure oil fluxes of PVDF/GE memberanes with different GE contents are shown in Figure 10a. The flux gradually increased with increasing GE content. When GE content was 3 wt %, it reached the maximum of 1671.97 L/m$^2$·h. As the GE content continued to increase, the flux became smaller. The flux of pure oil continued to be measured under the condition of changed coagulation bath. The flux of pure oil exhibited the best result when the coagulation bath was DOP, reaching 2484.08 L/m$^2$·h, as seen from Figure 10b. This is related to the oil channels observed in Figure 3. It shows that the changed coagulation bath could effectively improve the separation performance and flux of membranes. Figure S2 shows the lipophilicity of the membranes formed in different coagulation baths. The shorter the time, the better the lipophilicity. As shown in the figure, the membrane formed in DOP has the best lipophilicity, followed by hot water and cold water. However, the flux diagram shows that the flux of cold water was greater than that of hot water. Therefore, the pore size distribution of the membranes formed in cold and hot water was measured, and

the average pore diameter of hot water was smaller than that of cold water, as seen in Figure S3. This explained why the flux of hot water was always less than the flux of cold water.

Because oil was less dense than water, there must be oil slicks in oily wastewater. To solve this problem, the oil slick flux of the PVDF/GE membrane was characterized. As shown in Figure 10a,b, the flux of the oil slick was approximately 1/2 that of the pure oil. It showed that the PVDF/GE membrane could also be used in the treatment of oil wastewater.

## 4. CONCLUSION

In summary, PVDF/GE membranes with good lipophilicity and pore structure were prepared with a simple method. The pore structure was adjusted by changing GE content and the coagulation bath. It was found that the addition of GE increases the thermal stability, hydrophobicity, and lipophilicity of the membrane to a certain extent. The prepared membranes had the best separation performance when graphene content was 3 wt % and the coagulation bath was DOP. The rejection rate reached more than 99%. In addition, the change of the coagulation bath increased the separation performance of oil-in-water emulsion by more than 2-fold. Therefore, the membrane was simple to prepare and had excellent performance and was an ideal material for the treatment of actual oily wastewater.

## ■ ASSOCIATED CONTENT

### ⓈⒾ Supporting Information

The Supporting Information is available free of charge at https://pubs.acs.org/doi/10.1021/acsomega.2c00764.

Porosity of PVDF/GE membranes (Table S1); peak temperatures $T_m$, enthalpies $\Delta H_m$, and apparent crystallinity ($X_m$) for melting transitions of pure PVDF and PVDF/GE membranes with different graphene contents and different coagulation bath (Table S2); temperature at 5 and 50% weightlessness of PVDF/GE and carbon residue rate at 600 °C (Table S3); temperature at 5 and 50% weightlessness of PVDF/GE in different coagulation bath and carbon residue rate at 600 °C (Table S4); bottom surface SEM and CSM images of PVDF/GE membrane (Figure S1); lipophilic of the membranes formed in different coagulation bath (Figure S2); pore size distribution of the membranes formed in cold and pore size distribution of the membranes formed in hot water (Figure S3) (PDF)

## ■ AUTHOR INFORMATION

### Corresponding Authors

**Kaikai Chen** − *School of Textiles and Fashion, Shanghai University of Engineering Science, Shanghai 201620, China;* ⓞ orcid.org/0000-0002-8429-2279; Email: chenkaikai@sues.edu.cn

**Changfa Xiao** − *School of Textiles and Fashion, Shanghai University of Engineering Science, Shanghai 201620, China;* ⓞ orcid.org/0000-0003-0614-7348; Email: xiaochanfa@163.com

### Authors

**Murong Yang** − *School of Materials Science and Engineering, and State Key Laboratory of Separation Membranes and Membrane Processes, Tiangong University, Tianjin 300387, China*

**Mianning Wang** − *School of Materials Science and Engineering, and State Key Laboratory of Separation Membranes and Membrane Processes, Tiangong University, Tianjin 300387, China*

**Huanhuan Chen** − *School of Textiles and Fashion, Shanghai University of Engineering Science, Shanghai 201620, China*

**Haoyang Ling** − *CAS Key Laboratory of Bio-inspired Materials and Interfacial Science, Technical Institute of Physics and Chemistry, Chinese Academy of Sciences, Beijing 100190, China*

**Wei Zhao** − *School of Materials Science and Engineering, and State Key Laboratory of Separation Membranes and Membrane Processes, Tiangong University, Tianjin 300387, China*

**Haihui Liu** − *School of Materials Science and Engineering, and State Key Laboratory of Separation Membranes and Membrane Processes, Tiangong University, Tianjin 300387, China*

Complete contact information is available at:
https://pubs.acs.org/10.1021/acsomega.2c00764

### Author Contributions

The manuscript was written through contributions of all authors. All authors have given approval to the final version of the manuscript.

### Notes

The authors declare no competing financial interest.

## ■ ACKNOWLEDGMENTS

## ■ REFERENCES

(1) Li, L.; Ding, L.; Tu, Z.; Wan, Y.; Clausse, D.; Lanoiselle, J.-L. Recovery of linseed oil dispersed within an oil-in-water emulsion using hydrophilic membrane by rotating disk filtration system. *J. Membr. Sci.* **2009**, *342* (1−2), 70−79.

(2) Zhong, J.; Sun, X.; Wang, C. Treatment of oily wastewater produced from refinery processes using flocculation and ceramic membrane filtration. *Sep. Purif.* **2003**, *32* (1−3), 93−98.

(3) Ma, Q.; Cheng, H.; Fane, A. G.; Wang, R.; Zhang, H. Recent development of advanced materials with special wettability for selective oil/water separation. *Mater. Vie.* **2016**, *12* (16), 2186−2202.

(4) Ge, J.; Shi, L. A.; Wang, Y. C.; Zhao, H. Y.; Yao, H. B.; Zhu, Y. B.; Zhang, Y.; Zhu, H. W.; Wu, H. A.; Yu, S. H. Joule-heated graphene-wrapped sponge enables fast clean-up of viscous crude-oil spill. *Nat. Nano.* **2017**, *12*, 434−440.

(5) Stokstad, E. Looking beyond the spill, Obama highlights long-term restoration. *Sci.* **2010**, *328*, 1618−2202.

(6) Fragouli, D.; Athanassiou, A. Oil spill recovery: Graphene heaters absorb faster. *Nat. Nano.* **2017**, *12*, 406−407.

(7) Liu, Y.; Zhan, B.; Zhang, K.; Kaya, C.; Stegmaier, T.; Han, Z.; Ren, L. On-demand oil/water separation of 3D Fe foam by controllable wettability. *Chem. Eng. J.* **2018**, *331*, 278−289.

(8) Xiao, J.; Lv, W.; Song, Y.; Zheng, Q. Graphene/nanofiber aerogels: Performance regulation towards multiple applications in dye adsorption and oil/water separation. *Chem. Eng. J.* **2018**, *338*, 202−210.

(9) Si, Y.; Chen, L.; Yang, F.; Guo, F.; Guo, Z. Stable Janus superhydrophilic/hydrophobic nickel foam for directional water transport. *J. Colloid Interface Sci.* **2018**, *509*, 346−352.

(10) Zhang, J.; Seeger, S. Polyester materials with superwetting silicone nanofilaments for oil/water separation and selective oil absorption. *Adv. Funct. Mater.* **2011**, *21* (24), 4699−4704.

(11) Yeber, M.; Paul, E.; Soto, C. Chemical and biological treatments to clean oily wastewater: optimization of the photocatalytic process using experimental design. *Desalination Water Treat.* **2012**, *47* (1−3), 295−299.

(12) Komives, C. F.; Lilley, E.; Russell, A. J. Biodegradation of pesticides in nonionic water-in-oil microemulsions of tween 85: Relationship between micelle structure and activity. *Biotechnol. Bioeng.* **1994**, *43*, 946−959.

(13) Huang, Q.; Han, X.; Mao, F.; Chi, Y.; Yan, J. Effect of the particle surface on oil recovery from petroleum sludge. *Energy Fuels* **2014**, *28*, 4480−4485.

(14) Chawaloesphosiya, N.; Mongkolnauwarat, J.; Prommajun, C.; Wongwailikhit, K.; Painmanakul, P. Treatment of cutting-oily wastewater by electrocoagulation-flotation (ECF) process: Modeling approach. *Environ. Eng. Res.* **2015**, *20* (4), 392−396.

(15) Ma, W.; Zhang, M.; Liu, Z.; Kang, M.; Huang, C.; Fu, G. Fabrication of highly durable and robust superhydrophobic-superoleophilic nanofibrous membranes based on a fluorine-free system for efficient oil/water separation. *J. Membr. Sci.* **2019**, *570*, 303−313.

(16) Deowan, S. A.; Galiano, F.; Hoinkis, J.; Johnson, D.; Altinkaya, S. A.; Gabriele, B.; Hilal, N.; Drioli, E.; Figoli, A. Novel low-fouling membrane bioreactor (MBR) for industrial wastewater treatment. *J. Membr. Sci.* **2016**, *510*, 524−532.

(17) Galiano, F.; Friha, I.; Deowan, S. A.; Hoinkis, J.; Xiaoyun, Y.; Johnson, D.; Mancuso, R.; Hilal, N.; Gabriele, B.; Sayadi, S.; Figoli, A. Novel low-fouling membranes from lab to pilot application in textile wastewater treatment. *J. Colloid Interface Sci.* **2018**, *515*, 208−220.

(18) Quintana, J. B.; Weiss, S.; Reemtsma, T. Pathways and metabolites of microbial degradation of selected acidic pharmaceutical

and their occurrence in municipal wastewater treated by a membrane bioreactor. *Water Res.* **2005**, *39* (12), 2654−2664.

(19) Wan, W.; Lin, Y.; Prakash, A.; Zhou, Y. Three-dimensional carbon-based architectures for oil remediation: from synthesis and modification to functionalization. *J. Mater.* **2016**, *4*, 18687−18705.

(20) Tao, M.; Xue, L.; Liu, F.; Jiang, L. An intelligent superwetting PVDF membrane showing switchable transport performance for oil/water separation. *Adv. Mater.* **2014**, *26* (18), 2943−2948.

(21) Obaid, M.; Barakat, N. A.M.; Fadali, O.A.; Motlak, M.; Almajid, A. A.; Khalil, K. A. Effective and reusable oil/water separation membranes based on modified polysulfone electrospun nanofiber mats. *Chem. Eng. J.* **2015**, *259*, 449−456.

(22) Richards, H. L.; Baker, P. G. L.; Iwuoha, E. Metal nanoparticle modified polysulfone membranes for use in wastewater treatment: A Critical Review. *J. Sur. Eng. Mater. Adv. Technol.* **2012**, *2* (3), 183−193.

(23) Jones, M. N. Membrane technology (serono symposium publications, volume 64). *FEBS Lett.* **1992**, *297* (3), 309−310.

(24) Lee, M. W.; An, S.; Latthe, S. S.; Lee, C.; Hong, S.; Yoon, S. S. Electrospun polystyrene nanofiber membrane with superhydrophobicity and superoleophilicity for selective separation of water and low viscous oil. *Appl. Mater.* **2013**, *5* (21), 10597−10604.

(25) Sadeghi, I.; Aroujalian, A.; Raisi, A.; Dabir, B.; Fathizadeh, M. Surface modification of polyethersulfone ultrafiltration membranes by corona air plasma for separation of oil/water emulsions. *J. Membr. Sci.* **2013**, *430*, 24−36.

(26) Ou, R.; Wei, J.; Jiang, L.; Simon, G. P.; Wang, H. Robust thermoresponsive polymer composite membrane with switchable superhydrophilicity and superhydrophobicity for efficient oil−water separation. *Environ. Sci. Technol.* **2016**, *50* (2), 906−914.

(27) Kota, A. K.; Kwon, G.; Choi, W.; Mabry, J. M.; Tuteja, A. Hygro-responsive membranes for effective oil−water separation. *Nat. Commun.* **2012**, *3* (1), 1025.

(28) Yan, L.; Yang, X.; Zhao, Y.; Wu, Y.; Motlhaletsi Moutloali, R.; Mamba, B. B.; Sorokin, P.; Shao, L. Bio-inspired mineral-hydrogel hybrid coating on hydrophobic PVDF membrane boosting oil/water emulsion separation. *Sep. Purif.* **2022**, *285*, 120383−120393.

(29) Leenaerts, O.; Partoens, B.; Peeters, F. M. Water on graphene: Hydrophobicity and dipole moment using density functional theory. *Phys. Rev., B Condens.* **2009**, *79* (23), 235440.

(30) Zhao, X.; Zhang, Q.; Chen, D.; Lu, P. Enhanced mechanical properties of graphene-based poly (vinyl alcohol) composites. *Macromolecules* **2010**, *43* (5), 2357−2363.

(31) Liang, J.; Xu, Y.; Huang, Y.; Zhang, L.; Wang, Y.; Ma, Y.; Li, F.; Guo, T.; Chen, Y. Infrared-Triggered actuators from graphene-based nanocomposites. *J. Phys. Chem. C* **2009**, *113* (22), 9921−9927.

(32) Asmatulu, R.; Ceylan, M.; Nuraje, N. Study of super-hydrophobic electrospun nanocomposite fibers for energy systems. *Langmuir* **2011**, *27* (2), 504−507.

(33) Wu, X.; Zhao, B.; Wang, L.; Zhang, Z.; Zhang, H.; Zhao, X.; Guo, X. Hydrophobic PVDF/graphene hybrid membrane for CO2 absorption in membrane contactor. *J. Membr. Sci.* **2016**, *520*, 120−129.

(34) Yuan, X.; Li, W.; Liu, H.; Han, N.; Zhang, X. A novel PVDF/graphene composite membrane based on electrospun nanofibrous film for oil/water emulsion separation. *Compos. Commun.* **2016**, *2*, 5−8.

(35) Zhang, T.; Xiao, C.; Zhao, J.; Liu, X.; Ji, D.; Zhang, H. One-step facile fabrication of PVDF/graphene composite nanofibrous membrane with enhanced oil affinity for highly efficient gravity-driven emulsified oil/water separation and selective oil absorption. *Sep. Purif.* **2021**, *254*, 117576.

(36) Yan, L.; Yang, X.; Zhang, Y.; Wu, Y.; Cheng, Z.; Darling, S. B.; Shao, L. Porous Janus materials with unique asymmetries and functionality. *Mater. Today* **2021**, *51*, 626−647.